NASA TECHNICAL NOTE

NASA TN D-4320

A REAL-GAS STUDY OF LOW-DENSITY WEDGE-INDUCED LAMINAR SEPARATION ON A HIGHLY COOLED BLUNT FLAT PLATE AT $M_\infty = 12$

by John B. Anders and C. L. W. Edwards

Langley Research Center
Langley Station, Hampton, Va.

NATIONAL AERONAUTICS AND SPACE ADMINISTRATION • WASHINGTON, D. C. • MARCH 1968

A REAL-GAS STUDY OF LOW-DENSITY WEDGE-INDUCED

LAMINAR SEPARATION ON A HIGHLY COOLED

BLUNT FLAT PLATE AT $M_\infty = 12$

By John B. Anders and C. L. W. Edwards

Langley Research Center
Langley Station, Hampton, Va.

NATIONAL AERONAUTICS AND SPACE ADMINISTRATION

A REAL-GAS STUDY OF LOW-DENSITY WEDGE-INDUCED
LAMINAR SEPARATION ON A HIGHLY COOLED
BLUNT FLAT PLATE AT $M_\infty = 12$

By John B. Anders and C. L. W. Edwards
Langley Research Center

SUMMARY

A study has been made of real-gas wedge-induced laminar separation. A series of experimental tests on a blunt flat plate with a trailing-edge flap was made at a free-stream Mach number of 12 and a free-stream Reynolds number of 10^4/ft (3.3×10^4/m). The tests were conducted for stagnation enthalpies ranging from 1465 Btu/lbm (3.41 MJ/kg) to 2030 Btu/lbm (4.73 MJ/kg). A calculation technique is developed to predict the chordwise extent of wedge-induced laminar separation and agrees reasonably well with the present real-gas experimental data. The computed effect of free-stream Reynolds number and total enthalpy on the extent of separation is demonstrated. Sample calculations are shown for equilibrium and frozen flow for a range of total enthalpies.

INTRODUCTION

The occurrence of laminar-boundary-layer separation on maneuverable reentry vehicles results in large changes in aerodynamic characteristics, heat transfer, and control forces. This problem has been studied by many investigators and much theoretical and experimental information exists on laminar separated flows. (See refs. 1 to 22.) However, all the theoretical investigations, and all the experimental investigations with the exception of Kuehn's work (refs. 23 and 24) have considered the fluid to be a perfect gas. Also, with the exception of Rogers and Berry (ref. 25) and Kuehn (refs. 23 and 24), only relatively high-density flows have been investigated, usually with local Reynolds numbers above 10^4. The higher kinetic energies of reentering vehicles are normally associated with the early low-density region of the flight path. Therefore, the regions of low density and high enthalpy are linked together for this application.

The extension of present theories to low-density real-gas conditions invariably seems to violate assumptions made in their development. Similarly, the extrapolation of experimental results to low-density real-gas conditions is, perhaps, unfounded without some experimental investigation in this region. The present study was begun to check

experimentally certain semiempirical perfect-gas relations in the real-gas region and to see whether certain gross predictions of low-density real-gas separation could be made by utilizing simple physical concepts. Such a study would be useful in demonstrating trends as well as pointing the way to future research.

The model chosen for this study was a blunt-nosed wing-flap combination. All experimental testing was done in the Langley 1-foot hypersonic arc tunnel at a nominal Mach number of 12 and a nominal free-stream Reynolds number per foot of 1.4×10^4 (4.59×10^4 per meter). The Knudsen number based on nose diameter was approximately 0.06.

SYMBOLS

A,B   constants in equations (6) and (7)

a   speed of sound

$$C = \frac{\mu_w T}{\mu T_w}$$

C_1, C_2, C_3 constants in equations (11), (12), and (13)

$C_{p,p}$ plateau pressure coefficient, $\dfrac{p_p - p_o}{q_o}$

$c_{f,o}$ local-skin-friction coefficient

d   model nose diameter

$$G = 1.7208 \frac{\gamma - 1}{2}\left(\frac{T_w}{T_t} + 0.3859\right)$$

H_o form factor

h   enthalpy

$h_{t,2}$ stagnation enthalpy at model nose

k   nose drag coefficient

k_1 constant in equation (19)

L   model length to wedge hinge line

2

l_{ds} length of dividing streamline

l_i length over which pressure rise to plateau takes place

M   Mach number

m,n   defined by equations (14a) and (14b)

p   static pressure

p_b bluntness induced pressure

$p_{t,2}$ stagnation pressure on model nose

Δp_v viscous induced pressure increment

q   dynamic pressure

R   specific gas constant

R_∞ Reynolds number per foot   (per 0.3048 meter)   based on free-stream conditions, $\dfrac{\rho_\infty V_\infty}{\mu_\infty}$

$R_{\infty,L}$ free-stream Reynolds number based on plate length, $\dfrac{\rho_\infty V_\infty L}{\mu_\infty}$

$R_{\infty,x}$ free-stream Reynolds number based on longitudinal distance

$R_{x,o}$ Reynolds number based on conditions at beginning of interaction, $\dfrac{\rho_o V_o x_o}{\mu_o}$

S^* distance variable from reference 9

T   temperature

u^* velocity ratio along dividing streamline, $\dfrac{V}{V_2}$

V   velocity component

x   longitudinal coordinate (see fig. 2)

z	real-gas compressibility factor

$$\beta = \sqrt{M^2 - 1}$$

γ	ratio of specific heat
δ	angle of dividing streamline with plate surface (see fig. 10)
δ^*	displacement thickness
ϵ	function of γ, $\epsilon \approx 1 - \dfrac{0.0048}{(\gamma - 1)^2}$
θ	wedge deflection angle
μ	coefficient of viscosity
ξ	defined by equation (17)
ξ_1	correction factor in equations (4) and (5)
ρ	mass density of air
ϕ	defined by equation (18)
$\bar{\chi}_\infty$	viscous interaction parameter, $\dfrac{M_\infty^3 \sqrt{C_\infty}}{\sqrt{R_{\infty,x}}}$

Subscripts:

aw	adiabatic wall
c	computed value
o	condition at beginning of interaction
p	condition in plateau region
r	condition at reattachment
s	condition at separation

4

t	stagnation condition
w	condition on model wall
∞	free-stream condition
2	condition at edge of boundary layer

APPARATUS

The electric-arc-heated gas in the tunnel is expanded in a 5°-half-angle, conical nozzle to a nominal Mach number of 12. The inviscid core of this facility has been surveyed and was found to be approximately 5 inches (12.7 cm) in diameter. Test durations as long as 15 minutes have been utilized in this facility. A detailed description of the facility is presented in reference 26.

Model

The model used in the tests was a water-cooled, hemicylindrically blunted flat plate with a variable-angle trailing-edge flap. The plate had a nose radius of 1/8 inch (0.32 cm) and a chord of $2\frac{1}{2}$ inches (6.35 cm) and completely spanned the test section. The flap had a chord of $1\frac{1}{2}$ inches (3.81 cm) and a span of 4 inches (10.16 cm). The model was constructed of brass with a copper leading edge. The flap was designed for an angular variation of 20° to 45° and also for 0°. The model was also fitted with uncooled, detachable, stainless-steel end plates mounted 4 inches (10.16 cm) apart. A photograph of the model mounted in the test section is presented in figure 1. Figure 2 shows the end plates on the model and the position of the instrumentation. The model was instrumented with 4 chromel-alumel thermocouples and 31 pressure orifices. The pressure orifices were connected to ionization-type pressure sensors and both the thermocouple and ionization gage outputs were recorded on oscillograph film recorders.

Test Conditions

The present series of tests were conducted in air for a nominal Mach number of 12, a stagnation enthalpy range from 1465 Btu/lbm (3.41 MJ/kg) to 2030 Btu/lbm (4.73 MJ/kg), a free-stream Reynolds number per foot from 1.1×10^4 to 1.9×10^4 (3.6×10^4 per meter to 6.2×10^4 per meter), and a flap angle range from 27° to 32°. Tunnel blockage prevented flap angles larger than 32°. Precise values for tunnel conditions during specific tests are presented in table I. Ratios of wall temperature to total temperature varied from 0.11 for the lowest enthalpy test to 0.09 for the highest enthalpy test.
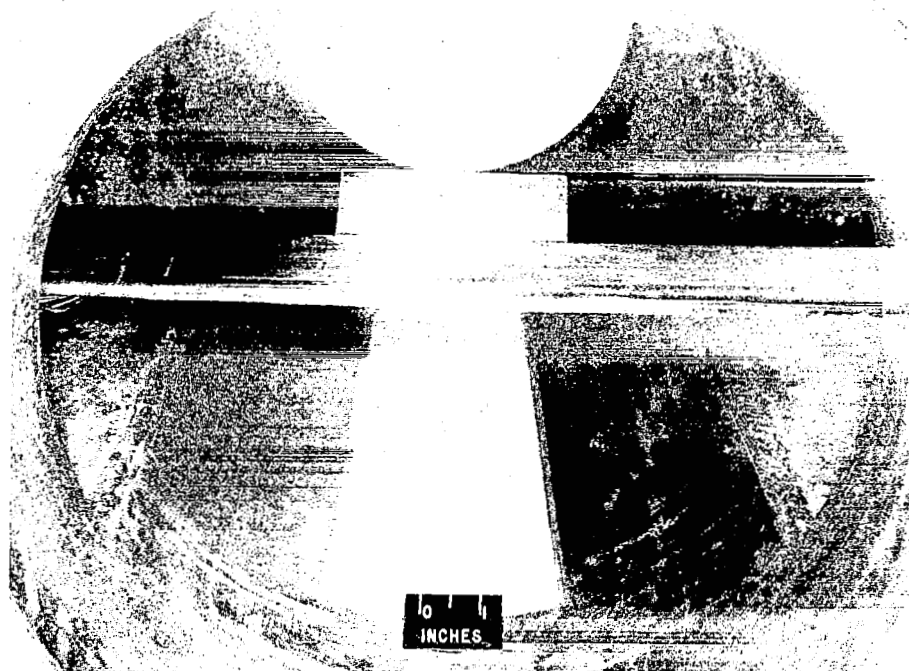
Figure 1.- Model installed in 1-foot test section. End plates removed.   L-67-8702

TABLE I.- TUNNEL TEST CONDITIONS

Test	h_t		p_t		p_∞		M_∞	R_∞		θ, deg
	Btu/lbm	MJ/kg	atm	N/m²	atm	N/m²		per foot	per meter	
1	1770	4.12	22.36	2.26×10^6	5.47×10^{-5}	5.54	12.4	1.5×10^4	4.9×10^4	27.0
2	2030	4.73	20.32	2.06	5.73	5.80	11.8	1.1	3.6	28.0
3	1619	3.77	22.22	2.25	5.09	5.16	12.7	1.8	5.9	30.5
4	1465	3.41	21.82	2.21	4.21	4.26	13.1	1.9	6.2	32.0
5	1850	4.31	21.82	2.21	5.58	5.65	12.2	1.4	4.6	31.0
6	1720	4.00	21.41	2.17	6.34	6.42	12.1	1.7	5.6	31.0
7	1950	4.54	21.17	2.14	5.96	6.04	11.9	1.2	4.9	31.0
8	1640	3.82	21.00	2.13	5.19	5.26	12.5	1.7	5.6	30.5
9	1998	4.65	21.37	2.16	5.62	5.70	12.0	1.1	3.6	30.5
10	1690	3.93	20.39	2.07	4.50	4.56	12.7	1.5	4.9	30.5
11	1830	4.26	18.62	1.89	5.84	5.92	11.9	1.3	4.3	30.5
12	1785	4.16	23.72	2.40	5.67	5.74	12.4	1.6	5.3	0

Pressure orifices	
No.	x/d
1	0
2	1.66
3	2.41
4	3.12
5	3.75
6	4.25
7	4.75
8	5.25
9	5.75
10	6.25
11	6.75
12	7.25
13	7.75
14	8.25
15	8.75
16	9.25
17	9.75
18	10.50
19	11.00
20	11.50
21	12.00
22	12.50
23	13.00
24	13.50
25	14.00
26	14.50
27	15.00
28	15.50
29	16.00
30	8.25
31	8.75

Thermo- couples	
No.	x/d
1	4.75
2	8.00
3	12.25
4	14.75

Pressure orifices

Thermocouples

Stagnation pressure tap

15.0 (38.1)

0.188 (0.478)

0.188 (0.478)

x

1.0 (2.54)

1.0 (2.54)

4.0 (10.16)

2.500 (6.350)

1.563 (3.969)

0.250 (0.635)

End plates

Variable angle flap
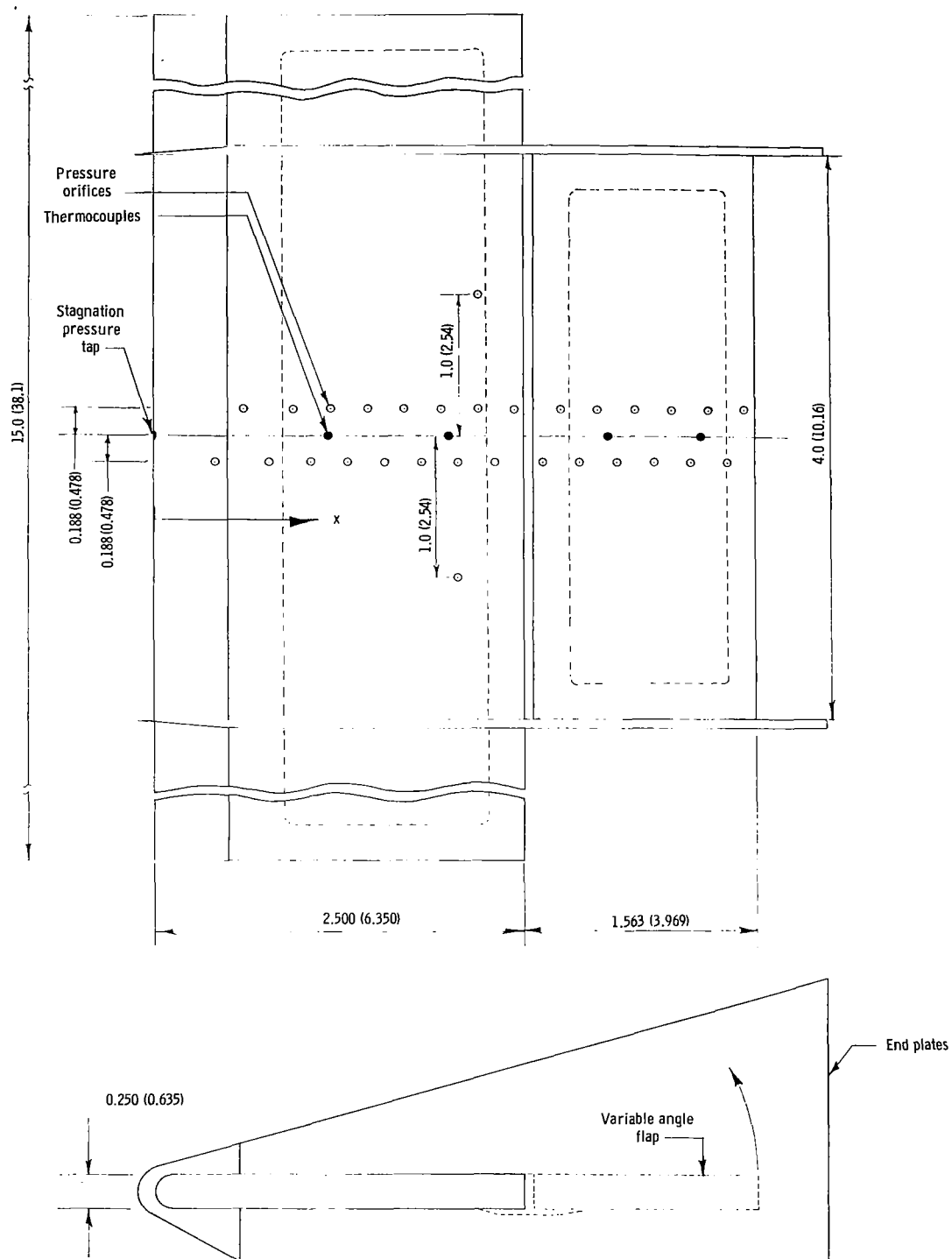
Figure 2.- Model schematic and instrumentation. (Dimensions are in inches (centimeters).)

Accuracy

The maximum error in determining the total enthalpy has been found to be about ±8 percent as reported in references 27 and 28. An orifice effect on pressure measurement has been investigated and reported in reference 29. This effect can cause a maximum error in pressure measurements of -6 percent for the lowest pressures measured in these tests. Maximum error due to the orifice effect on higher pressures such as those at separation, plateau, or reattachment is considerably less than -6 percent (usually less than 1 percent). A maximum inaccuracy in instrumentation and reading of data has been found to be ±5 percent. The total uncertainty for the lowest measured pressure is then 5 percent and -11 percent. This uncertainty in pressure causes an uncertainty in the calculation of local properties along the plate. Cases were calculated by using the maximum error in pressure and this procedure was found to result in a 2-percent deviation in $c_{f,0}$ and a 4-percent deviation in local Mach number. These deviations were considered to be insignificant in the overall results.

RESULTS AND DISCUSSION

Blunt-Plate Pressure Distribution Without Separation

Several tests were made with a 0° flap angle in order to determine the effect of the blunt nose on the pressure distribution over the plate. Figure 3 shows a typical measured pressure distribution with a 0° flap angle. No pressure measurements were made on the flap itself. Two theoretical distributions (refs. 30 and 31) are also shown. The method of Bertram and Blackstock (ref. 30) was found to give the best overall agreement with certain restrictions on γ. The method itself is not specifically valid for a variable γ flow; therefore, an attempt was made to represent the flow by some characteristic γ. Kuehn (ref. 32) discusses the use of a characteristic γ for blunt-nosed cylinders. He states that Wick of the NASA Ames Research Center has suggested that the value of γ at the stagnation region should be used since the blast analogy describes the flow in terms of a blast wave originating at the nose. In addition to the inviscid blast wave pressure, the viscous induced pressure must be taken into account; and intuitively, this viscous induced pressure might be characterized by a locally constant γ. From the analysis of reference 30, the inviscid and viscous pressures are given by the following expressions for Δp_V small compared with p_b

$$\frac{p_b}{p_\infty} = 0.187\epsilon \left[\sqrt{\gamma}(\gamma - 1) \frac{M_\infty^3 k}{x/d} \right]^{2/3} + 0.74 \tag{1}$$

and

$$\frac{\Delta p_V}{p_\infty} = \frac{5}{6} \frac{\gamma G \overline{\chi}_\infty}{\sqrt{p_b/p_\infty}} \tag{2}$$

where γ in equation (1) is now evaluated at the model stagnation point and γ in equation (2) is a local value evaluated at p_b and the stagnation-point entropy. The plate surface pressure is then given by

$$p_W = p_b + \Delta p_V \tag{3}$$

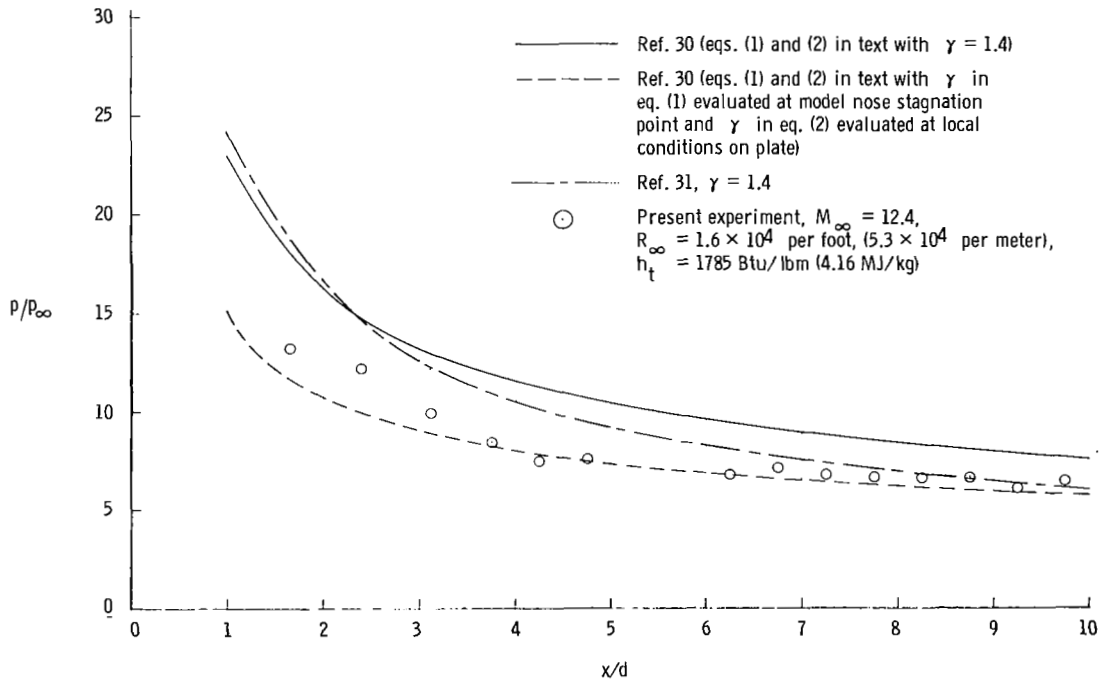These equations are used, without further qualification, for calculations presented later in this paper.

Figure 3.- Blunt-plate pressure distribution.

Separated Flow Results

Test data were obtained by two methods: oil-flow studies and pressure distributions. The partial-span flap of the present model leads to large three-dimensional effects in the separation bubble according to reference 33, and end plates were added to the model to minimize this spanwise bleed. A typical result from the addition of end plates is shown

9

in figure 4. The end plates significantly increased the chordwise extent of separation. With the exception of figure 4, all the data presented were taken with the end plates on and the effect of the end plates themselves is discussed in the light of the oil-flow patterns and spanwise pressure measurements.
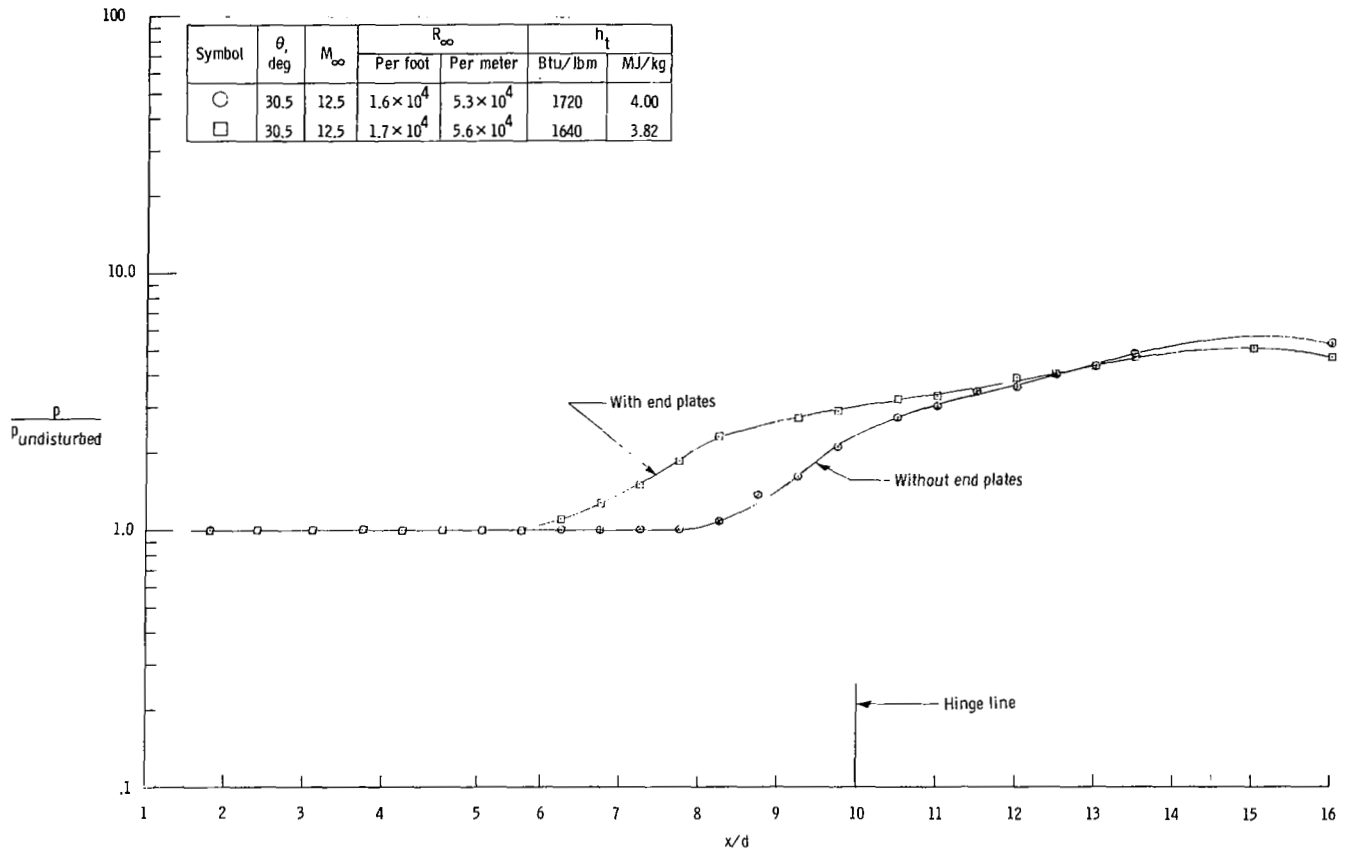
Symbol	θ, deg	M_∞	R_∞		h_t	
			Per foot	Per meter	Btu/lbm	MJ/kg
○	30.5	12.5	1.6×10^4	5.3×10^4	1720	4.00
□	30.5	12.5	1.7×10^4	5.6×10^4	1640	3.82

With end plates

Without end plates

Hinge line

Figure 4.- End-plate effect.

Oil-flow patterns.- The photographs of the oil-flow patterns were not of sufficient quality to warrant reproduction. However, figure 5 shows the pertinent features indicated by the original prints. Prior to a test, the surface of the plate was cleaned and dotted with drops of thin oil tinted with Prussian blue. The droplets were then observed during tunnel starting, approximately 2 minutes of testing time, and tunnel shutdown. The oil drops were observed to travel slowly back to a point on the plate surface, then to collapse and run together, and thus wet the plate surface. *The complete process occurred in 3 to 4 seconds and no change in the pattern could be detected during the remaining test time or during tunnel shutdown.* The forward edge of the wetted area was assumed to be the separation line and the position of this line is approximately halfway up the pressure rise to plateau pressure. However, on two of the oil-flow tests, the separated region was very

10

small and the pressure distributions did not exhibit a definite plateau. For these tests the oil-flow pattern indicated that separation occurred nearly three-fourths of the way up the pressure rise to the inflection point.

Spanwise pressure gradients.- All the oil-flow tests were made with end plates on, and from figure 5 the flow appears to be approximately two dimensional near the model center line. The oil streaks on either end of the model near the end plates curve inward slightly and indicate some end-plate effects in this region. Outboard pressure measurements were made to check for

Figure 5.- Sketch of typical oil-flow pattern.

any spanwise pressure gradients in the separated region not indicated by the oil streaks. Unfortunately, one outboard orifice developed a water leak at the onset of the test program and had to be plugged. The remaining outboard orifice indicated center-line pressure within the reading accuracy in 6 of the 11 tests. The other 5 tests indicated an outboard pressure 22 percent to 27 percent lower than the center line. This result might be expected since the separation pressure rise for most of the tests occurred near the outboard orifice. A slight spanwise variation in separation length could cause a fairly large variation in the pressure level sensed by the outboard orifice.

Chordwise pressure distributions.- Several typical pressure distributions are shown in figure 6, and table II lists the measured pressure distributions for all the tests. Figure 6 shows the effect of flap angle and also the nose bluntness effects on the pressures near the leading edge. Also shown is the calculated inviscid wedge pressure for each test. The short chord of the flap raises the question of whether reattachment is being affected by flap chord. Since the measured maximum flap pressure is very near the calculated inviscid values, it is assumed that the flap chord length is sufficient to insure a reattachment process free from flap chord effects. Also, calculations based on the technique presented later in this report indicate that reattachment should have occurred near the middle of the deflected flap for all except the 32° flap angle test. For the 32° test, reattachment appeared to occur at the top of the flap. In this instance the reattachment process was probably altered somewhat by the short flap chord.
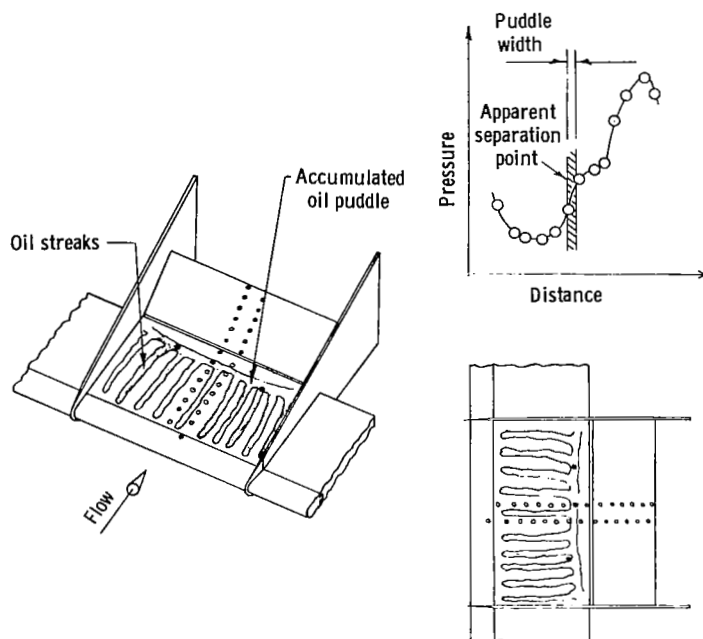
11

Symbol	θ, deg	M_∞	R_∞ Per foot	R_∞ Per meter	h_t Btu/lbm	h_t MJ/kg
○	27.0	12.4	1.5×10^4	4.9×10^4	1770	4.12
□	28.0	11.8	1.1	3.6×10^4	2030	4.73
◇	30.5	12.7	1.8	5.9×10^4	1619	3.77
△	32.0	13.1	1.9	6.2×10^4	1465	3.41

Inviscid wedge pressure for △

Inviscid wedge pressure for ◇

Inviscid wedge pressure for ○,□

Hinge line
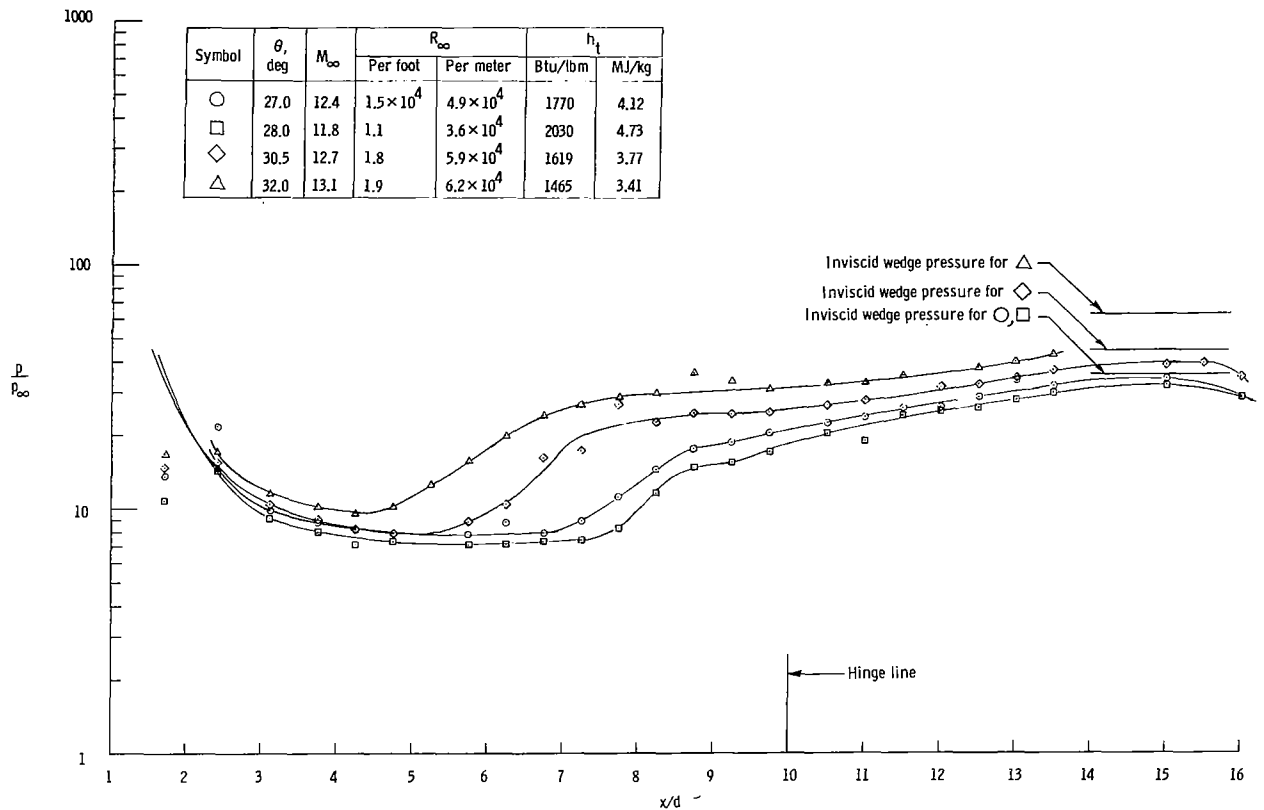
Figure 6.- Ratio of pressure to tunnel free-stream static pressure.

The pressure distributions were further reduced by expressing as a ratio the measured pressure to the pressure on the plate with a 0° flap. Where 0° flap pressure distributions were not available, extrapolated distributions obtained from the separated results were used. This type of data reduction allows a more meaningful comparison between tests as well as more clearly indicating the beginning of interaction. A typical plot of this type is shown in figure 7. The data for the 27° and 28° flap angles appear to show separation moving downstream with increasing flap angle. However, the 27° flap angle test had a higher Reynolds number and Mach number and a lower total enthalpy level and perhaps this fact accounts for the difference in the two tests. Nearly constant plateau regions were obtained in all the tests except those exhibiting only small separated regions. Rogers and Berry (ref. 25), in contrast to this result, did not find any evidence of a constant-pressure region in their investigation of low Reynolds number flow over a flat plate with forward-facing steps. The local Reynolds number on the plate for their tests ranged from 100 to 900 and indicated only a slight kink in the pressure distribution where plateau should have occurred. Gray (ref. 34) also questions the existence of a plateau in purely laminar flow. He indicates that this plateau is possibly a phenomenon

12

TABLE II.- MEASURED PRESSURE DISTRIBUTIONS

x/d	p/p_∞ for test —											
	1	2	3	4	5	6	7	8	9	10	11	12
0	209.0	193.1	218.5	234.4	204.0	199.0	195.0	213.0	198.0	219.1	192.6	209.3
1.66	13.58	10.80	14.74	17.50	20.17	11.62	11.59	12.95	12.18	14.61	14.98	13.30
2.41	21.75	14.37	15.50	17.80	13.33	11.84	11.15	12.31	11.36	13.75	13.64	12.20
3.12	9.85	9.20	10.33	12.19	9.55	8.61	8.50	9.90	8.90	10.09	9.57	10.00
3.75	8.77	8.05	9.04	10.62	8.26	7.26	7.50	10.91	7.96	9.06	9.12	8.40
4.25	8.17	7.13	8.27	10.00	7.55	6.74	6.74	7.62	7.02	8.19	8.00	7.50
4.75	7.94	7.36	7.88	10.62	7.43	6.33	6.84	9.14	7.15	5.85	8.11	7.60
5.25	-----	-----	-----	-----	-----	-----	-----	-----	-----	-----	-----	-----
5.75	7.81	7.13	8.78	16.25	5.56	6.43	6.62	7.74	7.26	-----	8.44	-----
6.25	8.78	7.13	10.33	20.62	7.43	6.02	6.62	7.62	6.67	7.60	7.55	6.80
6.75	7.94	7.36	16.02	25.00	8.60	-----	7.50	8.76	7.15	8.77	10.35	7.10
7.25	7.69	7.36	17.05	27.50	9.55	13.50	8.72	10.28	7.02	8.77	10.02	6.70
7.75	11.06	8.28	-----	29.70	12.85	7.26	12.03	12.81	8.32	11.40	10.93	6.60
8.25	14.30	11.50	22.23	30.61	16.15	11.00	15.12	15.86	10.89	14.48	12.74	6.60
8.75	17.43	14.70	24.30	37.20	18.51	11.63	16.90	-----	14.51	18.71	17.11	6.50
9.25	18.63	15.29	23.90	34.40	19.70	16.39	18.21	18.91	15.58	19.88	17.22	6.00
9.75	20.20	17.02	24.55	31.89	20.75	15.77	19.42	20.05	17.10	22.21	18.36	6.40
10.50	22.49	20.10	26.00	33.75	22.75	18.06	21.30	22.10	19.79	25.45	21.40	-----
11.00	23.56	19.30	27.40	34.10	23.70	22.81	21.20	23.00	20.95	26.31	22.63	-----
11.50	25.72	23.90	-----	36.26	21.81	19.92	18.21	18.40	23.30	29.25	25.00	-----
12.00	25.85	24.82	31.00	-----	27.95	25.00	26.05	27.18	25.30	31.58	25.80	-----
12.50	28.39	26.00	31.80	38.90	29.13	26.57	27.80	28.19	26.92	33.91	27.50	-----
13.00	33.18	27.70	33.86	41.25	41.85	28.42	29.80	30.08	28.34	35.68	29.40	-----
13.50	31.61	29.66	36.44	44.08	33.95	30.70	30.25	32.74	30.90	39.77	32.10	-----
14.00	-----	-----	-----	-----	-----	-----	-----	-----	-----	-----	-----	-----
14.50	-----	-----	-----	-----	-----	-----	-----	-----	-----	-----	-----	-----
15.00	33.06	31.86	38.00	-----	36.80	34.02	35.20	35.16	34.79	41.95	35.27	-----
15.50	-----	-----	-----	-----	-----	-----	-----	-----	-----	-----	-----	-----
16.00	28.00	28.30	33.85	-----	33.38	31.10	30.12	32.00	31.72	38.60	32.56	-----

Symbol	θ, deg	M_∞	R_∞		h_t	
			Per foot	Per meter	Btu/lbm	MJ/kg
○	27.0	12.4	1.5×10^4	4.9×10^4	1770	4.12
□	28.0	11.8	1.1	3.6×10^4	2030	4.73
◇	30.5	12.7	1.8	5.9×10^4	1619	3.77
△	32.0	13.1	1.9	6.2×10^4	1465	3.41
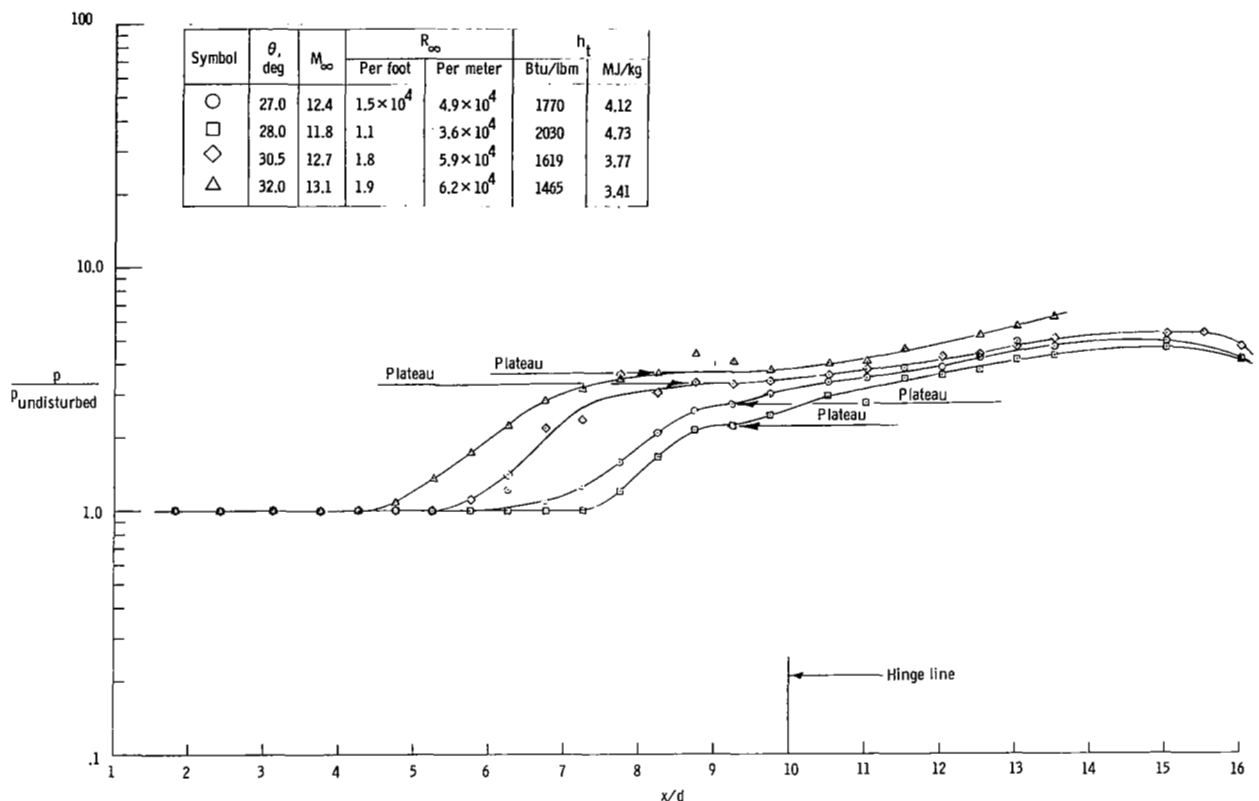
Figure 7.- Ratio of pressure to blunt flat-plate pressure without separation.

occurring only in transitional separated flows. The present tests were conducted at local plate Reynolds numbers of approximately 100 and, in most cases, exhibited a region of fairly constant pressure. It is doubtful that transition could be influencing these results at a Reynolds number this low.

Interaction length.- Figure 7 shows the values chosen to represent the constant-pressure plateau region. For those tests not having a definite plateau, the pressure at the inflection point near the hinge line was used. The interaction length is defined, for this report, as the chordwise distance over which the pressure rise to plateau takes place. This distance was determined from plots such as figure 7 and compared in figure 8 with a theoretical expression derived by Erdos and Pallone. (See ref. 35.) The expression presented in reference 35 gives the interaction length in terms of quantities at the beginning of interaction and has the form

$$\frac{l_i}{\delta_o{}^*} = \left[f_4(1)\right] \sqrt{\frac{2\xi_1}{\beta_o c_{f,o}}} \tag{4}$$

14
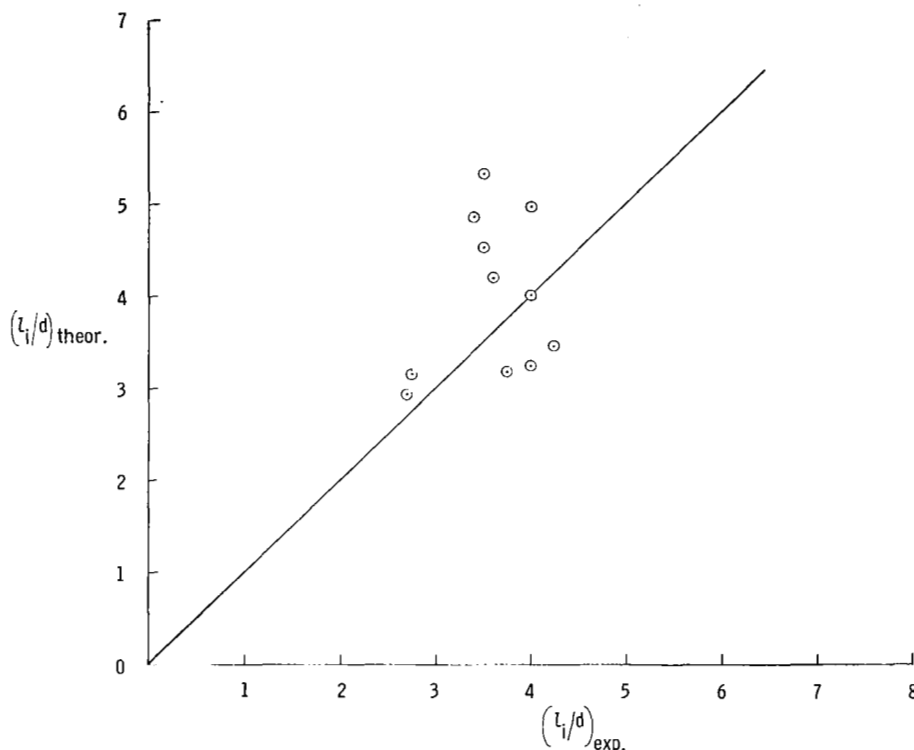
Figure 8.- Agreement between measured and predicted interaction length.

where $f_4(1)$ is empirically determined in reference 35 to be 3.43 for laminar flow, and ξ_1 is a correction factor to account for nonlinear effects at higher Mach numbers. For initial conditions (conditions at the interaction point) characterized by a flat-plate solution, equation (4) can be represented by

$$\frac{l_i}{x_o} = \frac{N}{N-1} \frac{H_o}{2} f_4(1) C_{p,p} \sqrt{\xi_1} \tag{5}$$

where for laminar flow $N = 2$ (from ref. 35). The form factor H_o was evaluated in reference 35 by using the expression given by Monaghan (ref. 36). For the comparison in figure 8, the direct effect of the pressure gradient near the nose on δ_o^* was neglected and equation (5) was used. The correction factor ξ_1 was assumed to be constant and determined by the best fit to the bulk of the experimental data. There is

15

considerable scatter about the line of perfect agreement. Perhaps this agreement could be improved by properly accounting for the effect of the history of the flow on the boundary-layer properties.

Comparison of the plateau pressure with theory.- Figure 9 shows the measured plateau pressure coefficients along with some of the other existing laminar separation data. The local Mach number and Reynolds number at the interaction point were calculated for the present tests by assuming an equilibrium isentropic expansion from the model nose. Calculations were also made for a flow frozen at the nose, but these calculations showed no appreciable change in $R_{x,o}$ and M_O from the equilibrium case.

The equation for the theoretical curves in figure 9 has been developed previously from linearized theory by several authors and has been experimentally verified at low Mach numbers. The equation has the form (ref. 8)

$$C_{p,p} = A\sqrt{\frac{2c_{f,o}}{\beta_o}} \tag{6}$$
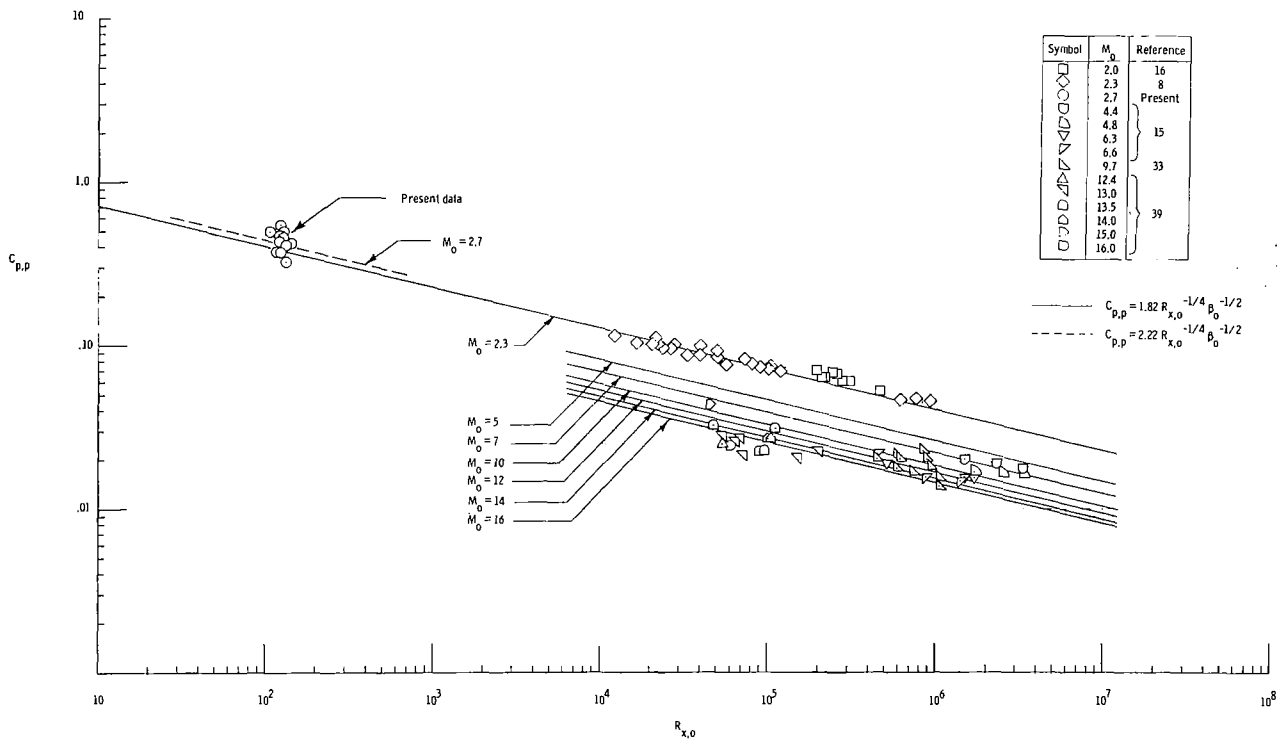
Figure 9.- Effect of Reynolds number on plateau pressure coefficient.

At low Mach numbers with moderate boundary-layer cooling and small pressure gradients, equation (6), for a flat plate, can be approximated by

$$C_{p,p} = B\left(R_{x,o}\right)^{-1/4}\left(\beta_o\right)^{-1/2} \tag{7}$$

The constants A and B have previously been evaluated empirically and the value for B suggested by Sterrett and Emery (ref. 14) to fit the data of reference 8 has been used in figure 9. Considerable disagreement with equation (7) is seen at the higher Mach numbers. The present data are at a low local Mach number and are in fair agreement with equation (7). An attempt was made to use the more exact form of equation (6) by computing a skin-friction coefficient by using the method of reference 37. The agreement with equation (6) offered no improvement over equation (7).

The present series of tests were conducted at a significantly higher stagnation enthalpy than the other data in figure 9. The introduction of this new variable may account for some of the scatter in the present data.

Calculated Results for Extent of Separation

The method described here allows the extent of laminar separation to be calculated with simplified physical concepts. This method is for wedge-induced separation where the separation and reattachment points are free to adjust themselves to changes in flow conditions and body geometry. Figure 10 illustrates the idealized flow model assumed for this method.

Assumptions.- Several assumptions are necessary in the development of this technique and these assumptions are:

(1) The pressure rises from interaction to plateau and from plateau to reattachment can be represented by oblique shocks

(2) The entropy gradient between the flow in the separated boundary layer and the inviscid flow can be neglected
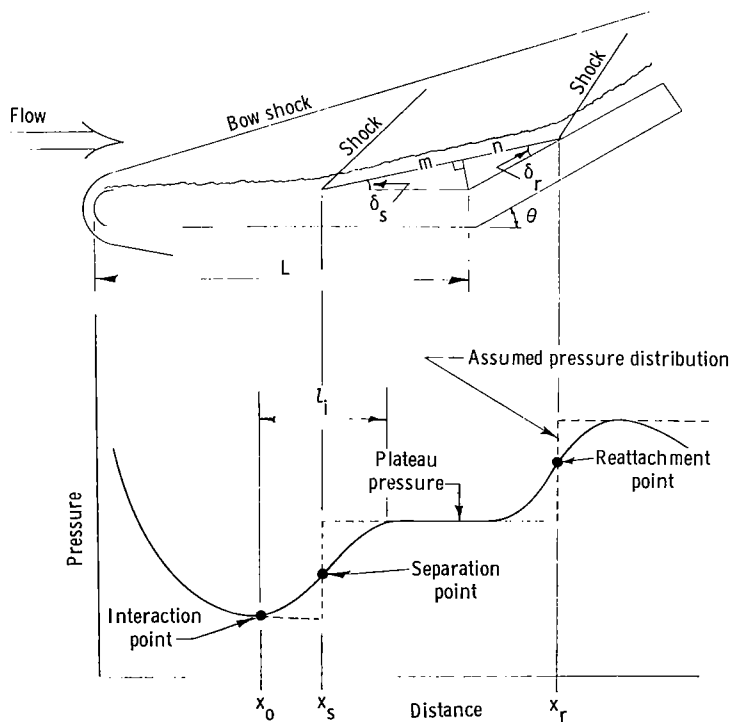
Figure 10.- Flow schematic and pressure distribution.

(3) The dividing streamline is straight

(4) The flow is parallel to the flap after reattachment

(5) The total pressure along the dividing streamline at reattachment is equal to the static pressure downstream of reattachment as proposed by Chapman, et al. (ref. 8)

(6) Separation occurs at the midpoint of the pressure rise to plateau pressure

(7) The plateau pressure coefficient is adequately predicted by equation (6)

(8) The interaction length is adequately predicted by equation (5).

Most of these assumptions are straightforward and have been discussed by other authors. However, some discussion is perhaps necessary on assumption (5). The assumption that the total pressure along the dividing streamline at reattachment is equal to the static pressure downstream of reattachment is now open to question (ref. 38); however, for the purpose of this paper, it is assumed that assumption (5) is valid. Chapman applied this idea to the case of zero initial shear layer thickness. More recently this work has been extended by Denison and Baum (ref. 9) and Kubota and Dewey (ref. 10) to include the non-similar growth of the free shear layer with finite initial thickness. It is these more recent results that are utilized in the present method to determine the reattachment pressure. Assumptions (6), (7), and (8) were examined experimentally and were discussed under the experimental tests.

For the purpose of discussion, the method can be divided into two parts: the region around the separation point and the region around the reattachment point. A detailed step-by-step procedure is presented in the appendix and frequent references to steps in this procedure are made.

Separation region.- When the flow properties at an assumed interaction point (see fig. 10) are known, the plateau pressure coefficient can be calculated by using equation (6). When $C_{p,p}$ and M_O are known, a flow deflection angle can be found by using oblique shock relations. For the case of a real gas, an iteration procedure (given by steps ㉚ to ㉕ in the appendix) is required to determine the flow-deflection angle. The interaction length l_i can be determined by equation (5). The separation point is then fixed by considering the pressure rise from p_O to p_S to be a mirror image of the pressure rise from p_S to p_p. Under these conditions, the separation point is given by

$$x_S = x_O + \frac{l_i}{2} \tag{8}$$

and the dividing stream leaves the plate surface at x_S with an angle δ_S.

Reattachment region.- The equation for p_r/p_p (shown in step ㊺ of the appendix) is taken from reference 8 and shows the reattachment or final pressure as a function

of γ, local Mach number, and the ratio of dividing streamline velocity to local free-stream velocity just prior to reattachment. The value of γ and Mach number are known since the pressure between separation and reattachment is assumed to be a constant. The only remaining unknown in the equation for p_r is u^*. References 9 and 10 provide graphs showing the variation of u^* with a distance parameter S^* for three different initial (separation point) profiles. The parameter S^* is evaluated, as in steps ㊷ and ㊸, for a particular flap angle θ and assumed interaction point. Then u^* can be taken directly from the graphs for any of the three initial profiles and p_r can be evaluated as in step ㊺. For all cases presented in this report, results from all three profiles are shown.

Once the reattachment pressure has been determined, the flow-deflection angle δ_r can be found from oblique shock relations. It is obvious from geometry that

$$\delta_s + \delta_r = \theta \tag{9}$$

Therefore, any solution must satisfy this equation, and a trial-and-error procedure is necessary to determine the correct flap angle for the assumed interaction point. The procedure in the appendix illustrates this trial-and-error technique.

Comparison and experiment.- Figure 11 shows a comparison of the calculated and experimental results for the extent of laminar separation. The results are better than might be expected from such a simplified approach to the problem. Since 0° flap tests were not available for all tests, the undisturbed, blunt-plate pressures used to determine flow properties at the edge of the boundary layer for the theoretical curves in figure 11 were obtained from the measured pressure distributions extrapolated to the plate-flap junction. The pressure gradient effect on skin friction was ignored and $c_{f,o}$ was computed by the Monaghan T' method. The plateau pressure coefficient was computed from equation (6). The exponential profile results seem to agree best with experiment.

All the calculated curves in figure 11 are for equilibrium flow with the exception of the two dashed curves shown in figures 11(a) and 11(c). These two cases were calculated for a flow frozen at the nose of the body. The frozen cases are seen to predict larger separated regions than the equilibrium cases at the same flap angle.

Since the results obtained from the calculation technique were in fair agreement with the experimental tests, several calculations at various enthalpy levels and free-stream unit Reynolds numbers were made. Two additional assumptions were necessary to compute these cases. First, the undisturbed, blunt-plate pressure was computed by the method of reference 30 by using equations (1) and (2). Second, the wall temperature was assumed to be constant at 300° K. The skin-friction coefficient and plateau pressure
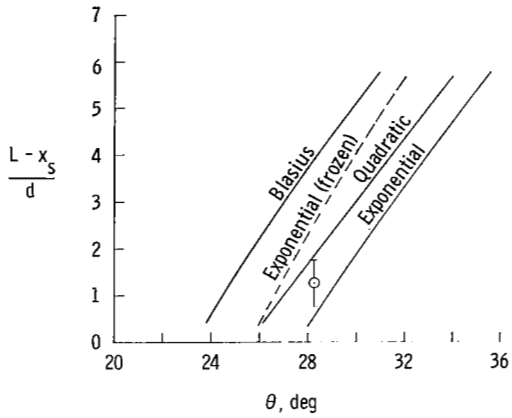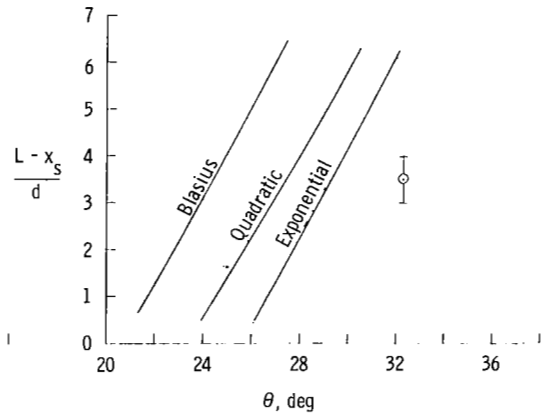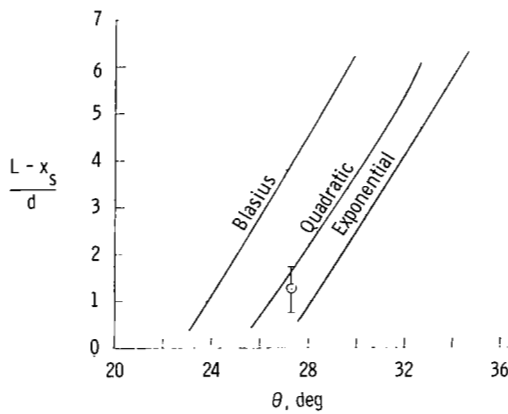
(a) $M_\infty = 11.8$; $h_t = 2030$ Btu/lbm (4.73 MJ/kg).
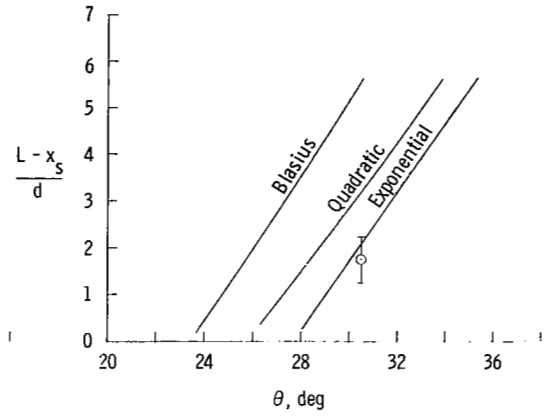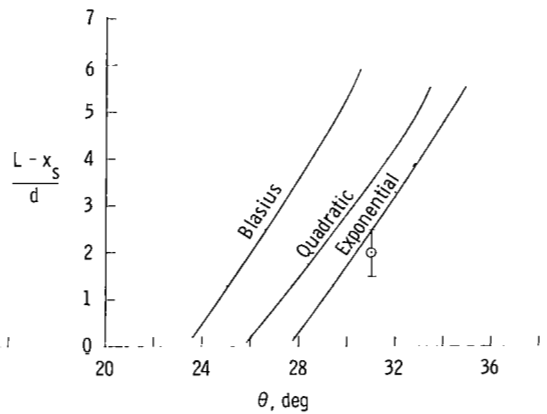
(b) $M_\infty = 12.0$; $h_t = 2000$ Btu/lbm (4.66 MJ/kg).
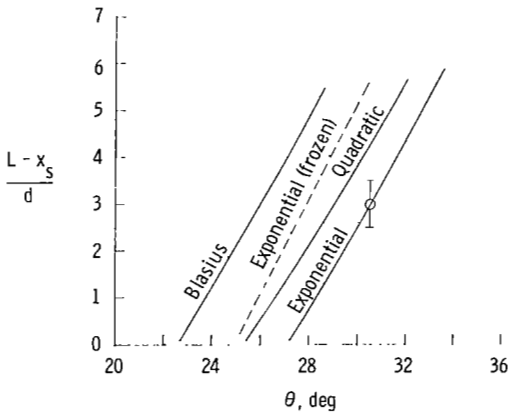
(c) $M_\infty = 12.7$; $h_t = 1619$ Btu/lbm (3.77 MJ/kg).
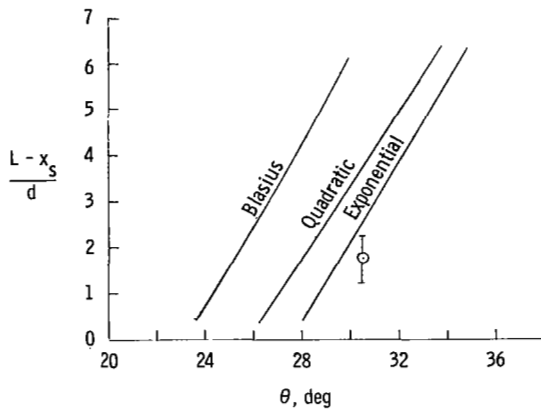
(d) $M_\infty = 13.1$; $h_t = 1465$ Btu/lbm (3.41 MJ/kg).
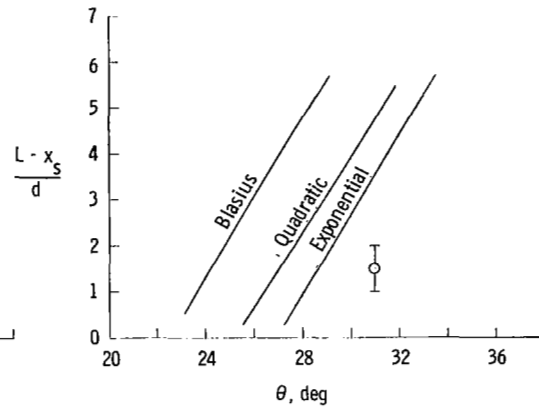
(e) $M_\infty = 12.4$; $h_t = 1770$ Btu/lbm (4.12 MJ/kg).
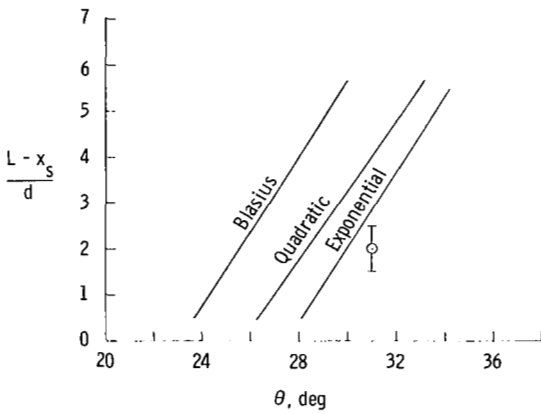
(f) $M_\infty = 11.9$; $h_t = 1950$ Btu/lbm (4.54 MJ/kg).

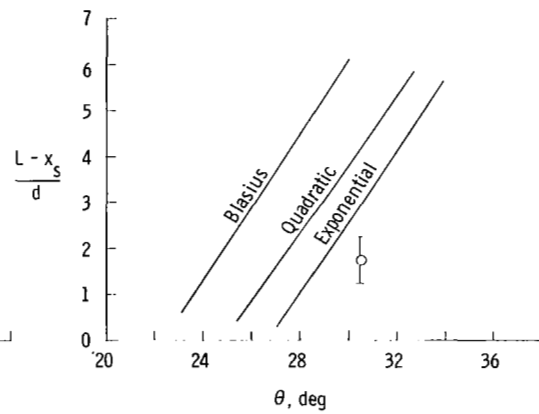Figure 11.- Variation of separation length with flap angle.

20

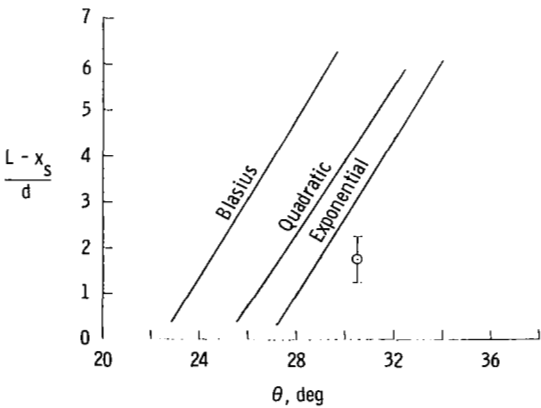(g) $M_\infty = 12.7$; $h_t = 1690$ Btu/lbm (3.94 MJ/kg).

(h) $M_\infty = 12.1$; $h_t = 1720$ Btu/lbm (4.01 MJ/kg).

(i) $M_\infty = 12.2$; $h_t = 1850$ Btu/lbm (4.31 MJ/kg).

(j) $M_\infty = 11.9$; $h_t = 1830$ Btu/lbm (4.26 MJ/kg).

(k) $M_\infty = 12.5$; $h_t = 1640$ Btu/lbm (3.82 MJ/kg).

Figure 11.- Concluded.

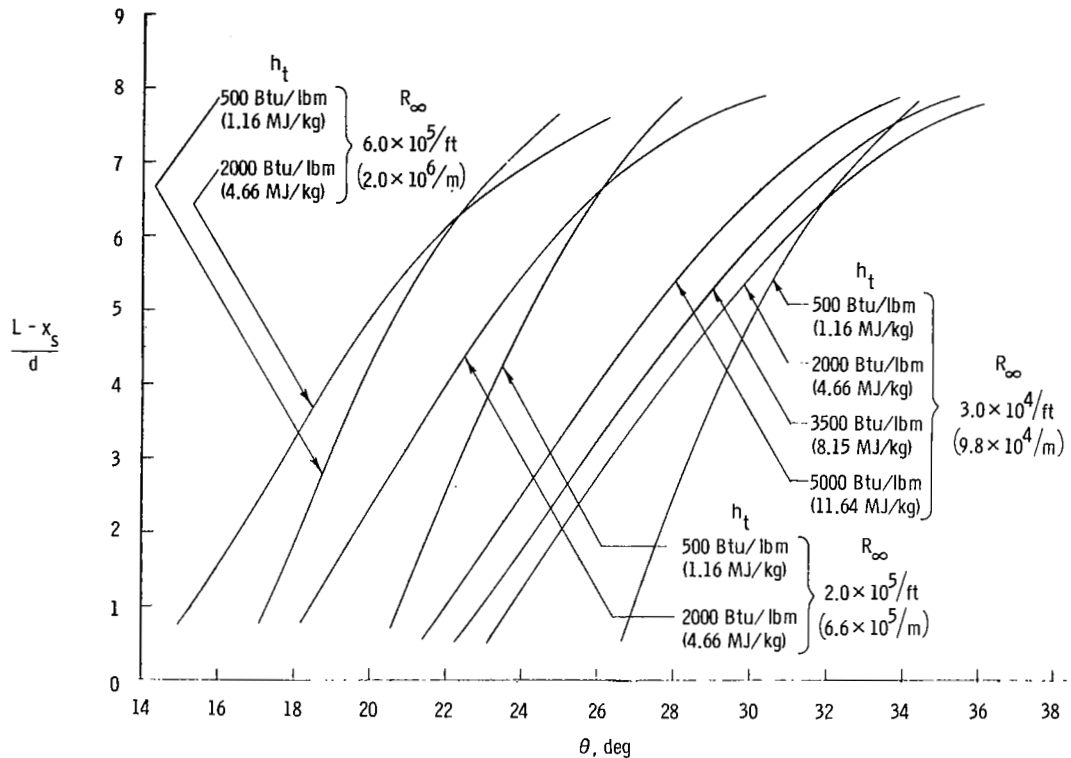Figure 12.- Effect of enthalpy on separation length. $M_\infty = 12.0$; $T_w = 300^\circ$ K.

coefficient were computed as before. Figure 12 shows the results of these calculations. This figure shows a large effect of free-stream unit Reynolds number and a smaller effect of enthalpy on separation distance.

Not shown are several cases computed at different free-stream Mach numbers $(10 < M_\infty < 20)$. Increasing the Mach number decreased the chordwise extent of laminar separation.

Correlation parameter for extent of separation.- The calculation technique just described has no closed-form expression for separation length. It would be helpful to see the manner in which the separation length depends on such variables as Mach number, Reynolds number, skin friction, and model geometry. An expression of this type may be derived from a relation taken from reference 8:

$$\frac{l_{ds}}{\delta_0{}^*} = \frac{1}{\sqrt{c_{f,0}}\sqrt{\beta_0}} \tag{10}$$

when

$$\delta_0{}^* = \frac{C_1 x_0}{\sqrt{R_{x,0}}} \tag{11}$$

$$c_{f,o} = \frac{C_2}{\sqrt{R_{x,o}}} \tag{12}$$

Equation (10) then reduces to

$$\frac{l_{ds}}{x_o} = C_3 \sqrt{\frac{c_{f,o}}{\beta_o}} \tag{13}$$

where

$$C_3 = \frac{C_1}{C_2}$$

Referring to figure 10 and assuming that $l_i/2$ can be neglected compared with l_{ds} yields

$$m = (L - x_o)\cos \delta_s \tag{14a}$$

$$n = \frac{(L - x_o)\sin \delta_s}{\tan(\theta - \delta_s)} \tag{14b}$$

$$l_{ds} = m + n = (L - x_o)\left[\cos \delta_s + \frac{\sin \delta_s}{\tan(\theta - \delta_s)}\right] \tag{15}$$

Combining equations (13) and (15) yields

$$\frac{L - x_o}{x_o} \propto \frac{\sqrt{c_{f,o}}}{\xi \sqrt{\beta_o}} \tag{16}$$

where

$$\xi = \cos \delta_s + \frac{\sin \delta_s}{\tan(\theta - \delta_s)} \tag{17}$$

The calculation technique (in the appendix) provides all the necessary information for evaluating the parameter on the right-hand side of equation (16) for a chosen inter-action point. Figure 13 shows a plot of equation (16) where

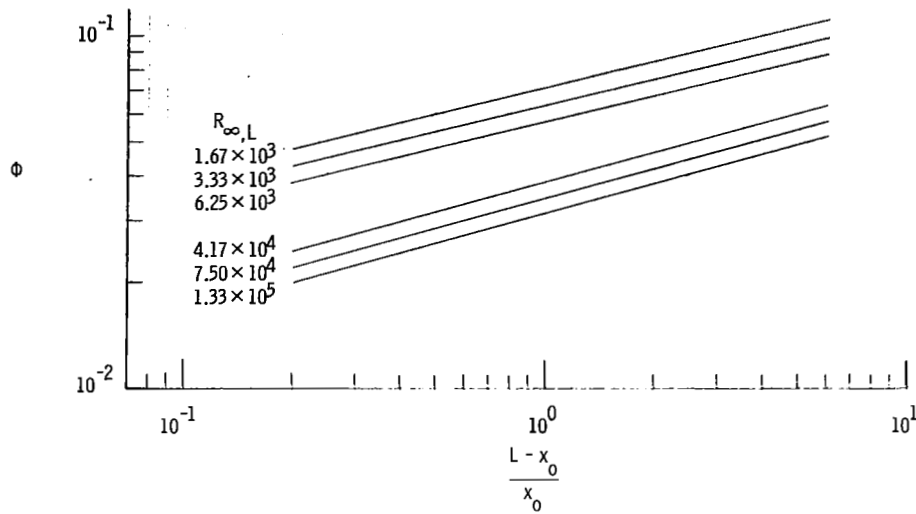$$\phi = \frac{\sqrt{c_{f,o}}}{\xi \sqrt{\beta_o}} \tag{18}$$

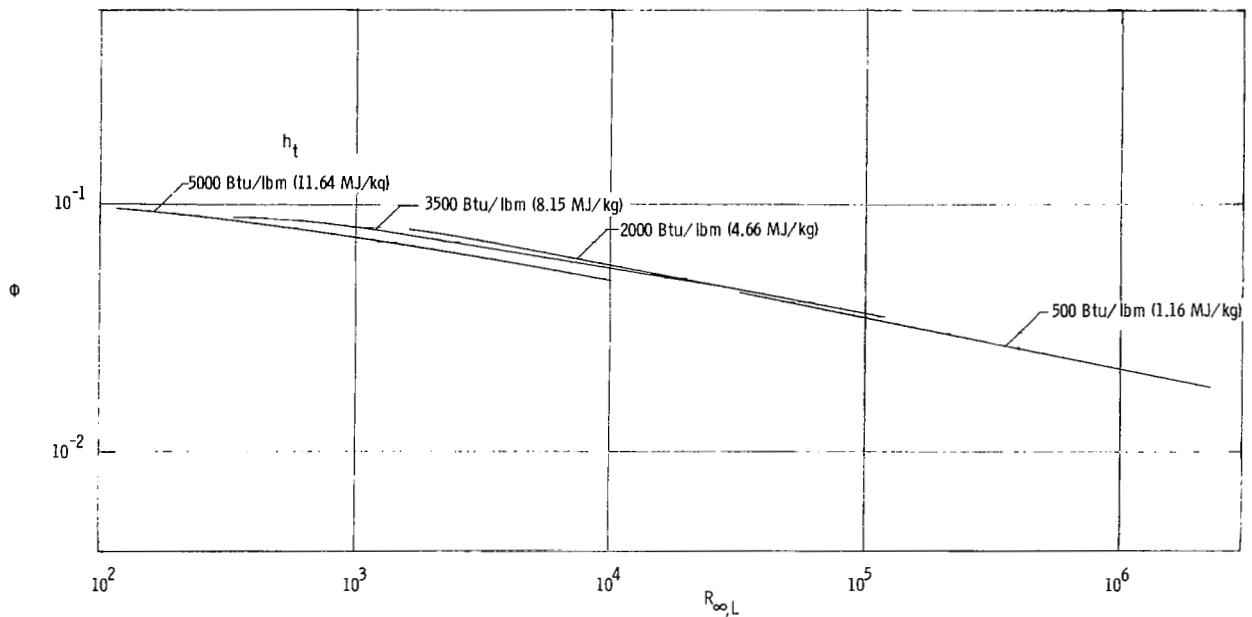Figure 13.- Correlation parameter. $M_\infty = 12.0$; $h_t = 2000$ Btu/lbm (4.66 MJ/kg).

Figure 14.- Effect of Reynolds number on Φ. $M_\infty = 12.0$; $\dfrac{(L - x_0)}{x_0} = 1.5$.

and ϕ is evaluated from the calculation technique (in the appendix) for several different free-stream Reynolds numbers based on plate length.

The term ϕ is seen to be not only a function of $(L - x_0)/x_0$ but also a function of $R_{\infty,L}$. This dependence is illustrated in figure 14 where ϕ is plotted against $R_{\infty,L}$ at constant $(L - x_0)/x_0$. Curves are shown for several different enthalpy levels. For 500 Btu/lbm $\leq h_t \leq$ 3500 Btu/lbm (1.16 MJ/kg $\leq h_t \leq$ 8.15 MJ/kg), and $10^3 \lesssim R_{\infty,L} \lesssim 10^6$, the calculated dependence of ϕ on $R_{\infty,L}$ can be approximated by

24

$$\phi \approx k_1 \left(R_{\infty, L}\right)^{-1/5} \qquad \left(\frac{L - x_O}{x_O} = \text{Constant}\right) \quad (19)$$

The 5000 Btu/lbm (11.65 MJ/kg) curve appears to be slightly displaced. Combining equation (19) with equation (16) gives

$$\phi\left(R_{\infty, L}\right)^{1/5} \propto \frac{L - x_O}{x_O} \qquad (20)$$

Figure 15 shows the variation of $\phi\left(R_{\infty, L}\right)^{1/5}$ with $\left(L - x_O\right)/x_O$. Equation (19) is an approximation, but for most practical purposes it may be assumed that the variation of $\phi\left(R_{\infty, L}\right)^{1/5}$ with $\left(L - x_O\right)/x_O$ reduces to a single curve for $10^3 \leq R_{\infty, L} \leq 10^6$ and 500 Btu/lbm $\leq h_t \leq 3500$ Btu/lbm $(1.16$ MJ/kg $\leq h_t \leq 8.15$ MJ/kg$)$.

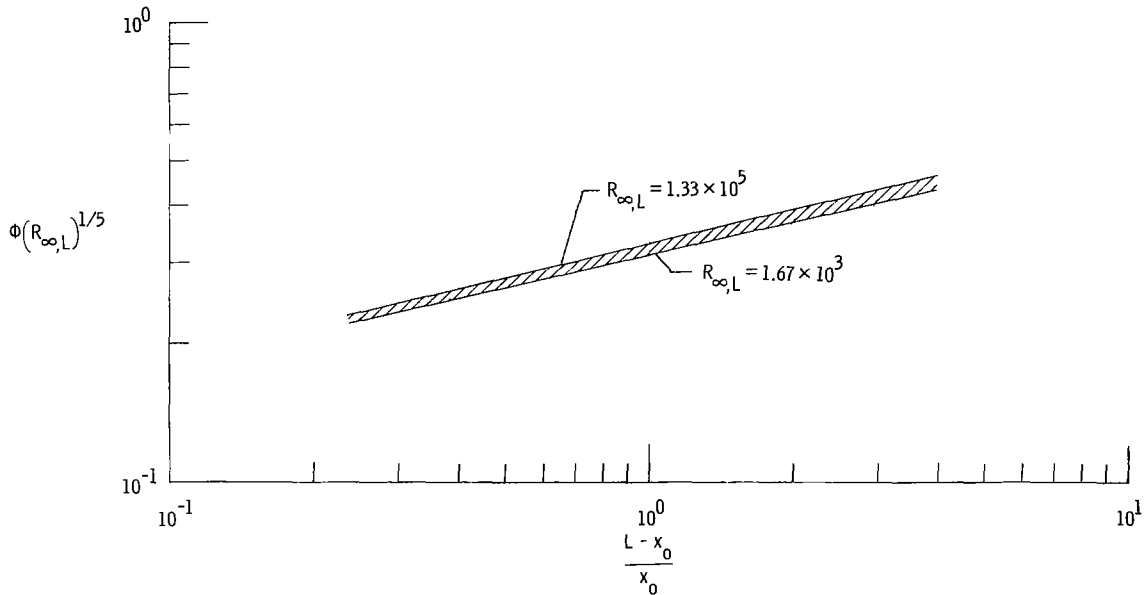
Figure 15.- Modified correlation parameter. $M_\infty = 12.0$; $h_t = 2000$ Btu/lbm (4.66 MJ/kg).

Figure 16 shows the present experimental data plotted in terms of the correlation parameter $\phi\left(R_{\infty, L}\right)^{1/5}$. The calculated curve was obtained from the calculation technique given in the appendix. Figure 16 also shows the sharp-plate data of Miller, et al. (ref. 39), Johnson (ref. 40), and Putnam (ref. 33). The dashed lines are faired through the experimental data. There appears to be an additional dependence on M_O. The trend with Reynolds number and Mach number is in agreement with linear separation theory and at constant M_O the experimental data correlate reasonably well even for various wall temperatures.
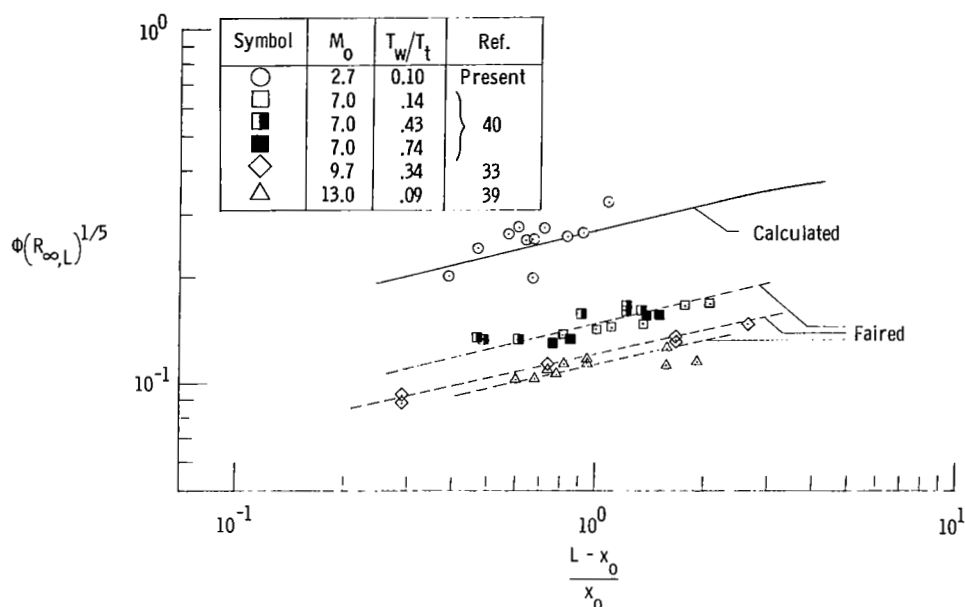
25

Figure 16.- Correlation of experimental data.

CONCLUDING REMARKS

A study has been made of real-gas wedge-induced laminar separation. A series of experimental tests were undertaken at a Mach number of 12 and Reynolds number per foot of 10^4 to establish the validity of a previously determined, perfect-gas relation for the plateau pressure coefficient. A calculation technique has been devised to predict the extent of wedge-induced, laminar separation utilizing simplified concepts.

The results of the study indicate that the previously determined relation for plateau pressure coefficient as a function of local Mach number and Reynolds number provides reasonable agreement with the present experimental data if real-gas conditions are used to evaluate local Mach number M_0 and Reynolds number $R_{x,0}$. The proposed calculation technique for the extent of wedge-induced laminar separation agrees reasonably well with the present, real-gas, experimental data. The results of calculations made by using this technique show that for laminar separation (a) increasing the Reynolds number per foot increases the chordwise extent of the separation region, (b) increasing enthalpy above 2000 Btu/lbm (4.66 MJ/kg) also increases the size of the separated region at the Reynolds numbers investigated, and (c) increasing free-stream Mach number decreases the extent of separation. A correlation parameter was developed which indicated a dependence of length of separation on local skin friction and Mach number and Reynolds number based on plate length. The parameter correlates with fair success

some previous, hypersonic separation data at several values of the ratio of wall temperature to total temperature. The trend of the results from the calculation technique developed here for the correlated length of separation agrees with linear separation theory and, for a blunted plate, agrees with the bulk of the present experimental data.

Langley Research Center,
    National Aeronautics and Space Administration,
        Langley Station, Hampton, Va., June 26, 1967,
            129-01-03-15-23.

APPENDIX

STEP-BY-STEP COMPUTATION PROCEDURE

This procedure shows the calculations necessary to compute the extent of wedge-induced laminar separation by the method outlined in this report. The procedure is suitable for real air in equilibrium. To start the calculations, it is assumed that columns (1) to (4) are given. The remaining columns are evaluated in turn. Figure 17 defines the pertinent quantities used in the calculations.
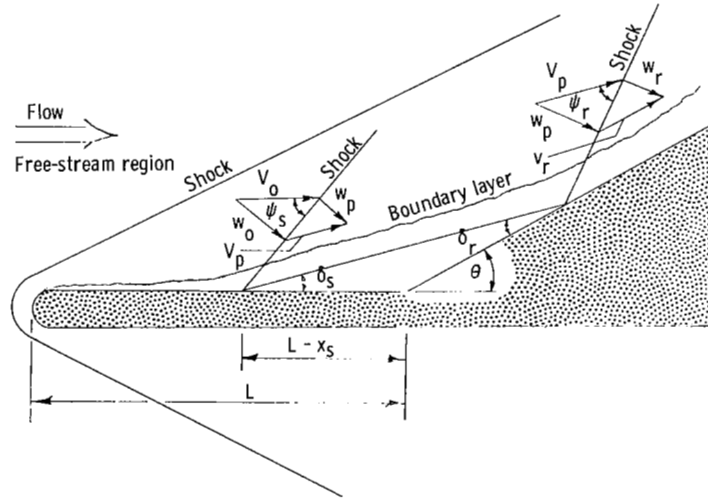
Figure 17.- Flow schematic showing velocity components.

Column	Heading	Definition
(1)	p_∞	free-stream pressure, lbf/ft^2 (N/m^2)
(2)	M_∞	free-stream Mach number
(3)	$p_{t,2}$	stagnation pressure, lbf/ft^2 (N/m^2) on model nose
(4)	$h_{t,2}$	stagnation enthalpy, Btu/lbm (J/kg) on model nose
(5)	p_2	plate surface pressure prior to separation, lbf/ft^2 (N/m^2) (calculated by method of ref. 30 for this paper)

APPENDIX

Column	Heading	Definition
⑥	h_2	local value of static enthalpy at edge of boundary layer, Btu/lbm (J/kg)
⑦	T_2	local value of static temperature at edge of boundary layer, $^\circ R$
⑧	ρ_2	local value of density at edge of boundary layer, slugs/ft^3 (kg/m^3)
⑨	a_2	local value of speed of sound at edge of boundary layer, fps (m/s) $\left(\text{⑥, ⑦, ⑧, and ⑨ may be computed by isentropic expansion from } p_{t,2} \text{ to } p_2 \text{ on thermodynamic charts, refs. 41 to 44}\right)$
⑩	μ_2	local viscosity at edge of boundary layer from reference 42 at p_2 and T_2, lbf-sec/ft^2 (N-sec/m^2)
⑪	V_2	local velocity at edge of boundary layer, $\sqrt{2\left(h_{t,2} - h_2\right)}$ or $\sqrt{2\left(④ - ⑥\right)}$ (Use appropriate units.)
⑫	x_0	distance from model nose to beginning of pressure rise to plateau, ft (m). A value of x_0 is chosen and calculations yield correct flap angle for this x_0.
⑬	$R_{x,o}$	local Reynolds number, $\dfrac{\rho_o V_o x_o}{\mu_o}$ or $\dfrac{⑧\,⑪\,⑫}{⑩}$ where zero subscript quantities are local values obtained in steps ⑤ to ⑪ at the chosen x_0
⑭	M_0	local Mach number at x_0, $\dfrac{V_o}{a_o}$ or $\dfrac{⑪}{⑨}$
⑮	β_0	$\beta_o = \sqrt{M_o{}^2 - 1} = \sqrt{⑭{}^2 - 1}$
⑯	$c_{f,o}$	local-skin-friction coefficient at x_0 (calculated by Monaghan T' method for this paper)
⑰	q_0	$\frac{1}{2}\rho_o V_o{}^2$ or $\frac{1}{2}⑧\,⑪{}^2$, lbf/ft^2 (N/m^2)

APPENDIX

Column	Heading	Definition
⑱	$C_{p,p}$	plateau pressure coefficient at x_O, $\dfrac{p_p - p_O}{q_O}$, $1.58\sqrt{\dfrac{2c_{f,o}}{\beta_O}}$ or $1.58\sqrt{\dfrac{2\,⑯}{⑮}}$
⑲	p_p	plateau pressure, $C_{p,p}q_O + p_O$ or $⑱\,⑰ + ⑤$, lbf/ft^2 (N/m^2)
⑳	w_p/w_o	normal velocity ratio defined in figure 17. A value of this ratio is assumed.
㉑	h_p	static enthalpy in plateau region, $h_O + \dfrac{p_p - p_O}{2\rho_O}\left(1 + \dfrac{w_p}{w_o}\right)$ or $⑥ + \dfrac{⑲ - ⑤}{2\,⑧}\left(1 + ⑳\right)$, Btu/lbm (J/kg)
㉒	z_p	local value of compressibility factor in plateau region from thermodynamic charts at p_p and h_p
㉓	T_p	local value of temperature in plateau region from thermodynamic charts at p_p and h_p, $^\circ R$
㉔	ρ_p	local value of density in plateau region at p_p and T_p, $\dfrac{p_p}{z_p R T_p}$ or $\dfrac{⑲}{㉒ R ㉓}$, $slugs/ft^3$ (kg/m^3)
㉕	ρ_o/ρ_p	density ratio across oblique shock, $\dfrac{⑧}{㉔}$. If $㉕ = ⑳$, then ρ_p is correct. If $㉕ \neq ⑳$, then a new value of w_p/w_o in ⑳ must be assumed and steps ㉑ to ㉕ repeated until $⑳ = ㉕$.
㉖	w_o	velocity component defined in figure 17, $\sqrt{\dfrac{2(h_p - h_o)}{1 - \left(w_p/w_o\right)^2}}$ or $\sqrt{\dfrac{2(㉑ - ⑥)}{1 - ⑳^2}}$, fps (m/s)
㉗	ψ_s	shock angle defined in figure 17, $\arcsin w_o/V_o$ or $\arcsin ㉖/⑪$
㉘	δ_s	separation angle defined in figure 17, $\psi_s - \arctan\left[(\tan \psi_s)(w_p/w_o)\right]$ or $㉗ - \arctan\left[(\tan ㉗)\,⑳\right]$

Column	Heading	Definition

㉙ V_p

local velocity at edge of boundary layer in plateau region as defined in figure 17, $\dfrac{w_p}{\sin(\psi_s - \delta_s)}$ or $\dfrac{㉚㉖}{\sin(㉗ - ㉘)}$, fps (m/s)

㉚ γ_p

ratio of specific heats evaluated at p_p and T_p

㉛ μ_p

local viscosity in plateau region from reference 42 at p_p and T_p, (lbf-sec/ft^2) (N-sec/m^2)

㉜ a_p

local speed of sound in plateau region, $\sqrt{\gamma_p z_p T_p R}$ or $\sqrt{㉚㉒㉓ R}$, fps (m/s)

㉝ M_p

local Mach number in plateau region, $\dfrac{V_p}{a_p}$ or $\dfrac{㉙}{㉜}$

㉞ $T_{w,o}$

plate surface temperature at x_o, $^{\circ}R$

㉟ $T_{aw,o}$

adiabatic wall temperature at x_o, $^{\circ}R$

㊱ H_o

form factor at x_o, $\delta_o{}^*/\theta_o$. Reference 35 suggests that H_o be calculated by $2.59\left[1 + 1.20\left(\dfrac{T_{w,o}}{T_o} - 1\right) + 0.4\left(\dfrac{T_{aw,o}}{T_o} - 1\right)\right]$

or $2.59\left[1 + 1.20\left(\dfrac{㉞}{⑦} - 1\right) + 0.4\left(\dfrac{㉟}{⑦} - 1\right)\right]$

㊲ l_i

interaction length defined in figure 10, $3.43 x_o H_o \sqrt{\dfrac{2c_{f,o}}{\beta_o}}\sqrt{\xi_1}$ (from ref. 35) or $3.43\,⑫㊱\sqrt{\dfrac{2⑯}{⑮}}\sqrt{\xi_1}$, ft (m)

㊳ x_s

distance from model nose to separation point, $x_o + \dfrac{l_i}{2}$ or $⑫ + \dfrac{1}{2}㊲$, ft (m)

㊴ L

distance from model nose to hinge line, ft (m)

㊵ $L - x_s$

distance from hinge line to separation point, $㊴ - ㊳$, ft (m)

Column	Heading	Definition

$\textcircled{41}$ θ wedge angle defined in figure 17. θ must be assumed and the following calculations done to determine whether the assumed θ is correct for the chosen x_0.

$\textcircled{42}$ x_{ds} length of dividing streamline, $(L - x_s)\cos \delta_s + \dfrac{(L - x_s)\sin \delta_s}{\tan(\theta - \delta_s)}$

or $\textcircled{40} \cos \textcircled{28} + \dfrac{\textcircled{40} \sin \textcircled{28}}{\tan\left(\textcircled{41} - \textcircled{28}\right)}$, ft (m)

$\textcircled{43}$ s^* distance parameter from reference 9, $\left(\dfrac{0.11\rho_p V_p \mu_p}{\displaystyle\int_0^{x_s} \rho_2 V_2 \mu_2 \, dx}\right) x_{ds}$

or $\left(\dfrac{0.11\,\textcircled{24}\,\textcircled{29}\,\textcircled{31}}{\displaystyle\sum_{x=0}^{x=x_s} \textcircled{8}\,\textcircled{11}\,\textcircled{10}\,\Delta x}\right)\textcircled{42}$. The step size Δx is chosen for desired accuracy or the denominator may be evaluated graphically.

$\textcircled{44}$ u^* velocity ratio along dividing streamline from reference 10

$\textcircled{45}$ p_r / p_p pressure ratio across reattachment region (from ref. 8),

$$\left[\dfrac{1 + \dfrac{\gamma_p - 1}{2} M_p^2}{1 + \left(1 - u^{*2}\right)\dfrac{\gamma_p - 1}{2} M_p^2}\right]^{\frac{\gamma_p}{\gamma_p - 1}} \quad \text{or}$$

$$\left[\dfrac{1 + \dfrac{\textcircled{30} - 1}{2} \textcircled{33}^2}{1 + \left(1 - \textcircled{44}^2\right)\left(\dfrac{\textcircled{30} - 1}{2}\right)\textcircled{33}^2}\right]^{\frac{\textcircled{30}}{\textcircled{30} - 1}}$$

$\textcircled{46}$ p_r reattachment pressure, $\textcircled{45}\,\textcircled{19}$, lbf/ft^2 (N/m^2)

Column	Heading	Definition
㊼	w_r/w_p	normal velocity ratio defined in figure 17. A value of this ratio is assumed.
㊽	h_r	
㊾	z_r	
㊿	T_r	The same procedure as used in steps ㉑ to ㉕ is repeated for steps ㊽ to ㊿ until ㊼ is equal to ㊼
㊉	ρ_r	
㊌	ρ_p/ρ_r	

㊽ to ㊾ definitions bracketed together: The same procedure as used in steps ㉑ to ㉕ is repeated for steps ㊽ to ㊒ until ㊼ is equal to ㊒

㊓	ψ_r	shock angle defined in figure 17, $\arc \sin w_p/V_p$ or $\arc \sin \dfrac{⑳㉖}{㉙}$
㊔	δ_r	reattachment angle defined in figure 17, $\psi_r - \arc \tan\left[\tan\psi_r\left(\dfrac{w_r}{w_p}\right)\right]$ or $⑬ - \arc \tan\left[(\tan⑬)㊼\right]$
㊕	θ_c	computed value of wedge angle, $\delta_s + \delta_r$ or $㉘ + ㊔$. If $㊕ = ㊇$, this solution is correct. If $㊕ \neq ㊇$, then a new value of θ in ㊇ must be assumed and steps ㊈ to ㊕ are repeated until $㊇ = ㊕$.

33

REFERENCES

1. Schlichting, Hermann: Boundary Layer Theory. McGraw-Hill Book Co., Inc., 1955.

2. Thwaites, B.: Approximate Calculation of the Laminar Boundary Layer. Aero. Quarterly, vol. I, Nov. 1949, pp. 245-280.

3. Makofski, R. A.: A Two-Parameter Method for Shock Wave-Laminar Boundary Layer Interaction and Flow Separation. Proceedings of the 1963 Heat Transfer and Fluid Mechanics Institute, Anatol Roshko, Bradford Sturtevant, and D. R. Bartz, editors, Stanford Univ. Press, c.1963, pp. 112-127.

4. Crocco, Luigi; and Lees, Lester: A Mixing Theory for the Interaction Between Dissipative Flows and Nearly Isentropic Streams. J. Aeron. Sci., vol. 19, no. 10, Oct. 1952, pp. 649-676.

5. Glick, Herbert S.: Modified Crocco-Lees Mixing Theory for Supersonic Separated and Reattaching Flows. J. Aerospace Sci., vol. 29, no. 10, Oct. 1962, pp. 1238-1249.

6. Tani, Itiro: On the Approximate Solution of the Laminar Boundary-Layer Equations. J. Aeron. Sci., vol. 21, no. 7, July 1954, pp. 487-495, 504.

7. Lees, Lester; and Reeves, Barry L.: Supersonic Separated and Reattaching Laminar Flows: I. General Theory and Application to Adiabatic Boundary-Layer/Shock-Wave Interactions. AIAA J., vol. 2, no. 11, Nov. 1964, pp. 1907-1920.

8. Chapman, Dean R.; Kuehn, Donald M.; and Larson, Howard K.: Investigation of Separated Flows in Supersonic and Subsonic Streams With Emphasis on the Effect of Transition. NACA Rept. 1356, 1958.

9. Denison, M. Richard; and Baum, Eric: Compressible Free Shear Layer With Finite Initial Thickness. AIAA J., vol. 1, no. 2, Feb. 1963, pp. 342-349.

10. Kubota, Toshi; and Dewey, C. Forbes, Jr.: Momentum Integral Methods for the Laminar Free Shear Layer. AIAA J., vol. 2, no. 4, Apr. 1964, pp. 625-629.

11. Gadd, G. E.: A Simple Theory for Interactions Between Shock Waves and Entirely Laminar Boundary Layers. J. Aeron. Sci., vol. 23, no. 3, Mar. 1956, pp. 225-230.

12. Gadd, G. E.: A Theoretical Investigation of Laminar Separation in Supersonic Flow. J. Aeron. Sci., vol. 24, no. 10, Oct. 1957, pp. 759-771.

13. Gadd, G. E.: Boundary Layer Separation in the Presence of Heat Transfer. AGARD Rept. 280, Apr. 1960.

14. Sterrett, James R.; and Emery, James C.: Extension of Boundary-Layer-Separation Criteria to a Mach Number of 6.5 by Utilizing Flat Plates With Forward-Facing Steps. NASA TN D-618, 1960.

15. Sterrett, James R.; and Emery, James C.: Experimental Separation Studies for Two-Dimensional Wedges and Curved Surfaces at Mach Numbers of 4.8 to 6.2. NASA TN D-1014, 1962.

16. Hakkinen, R. J.; Greber, I.; Trilling, L.; and Abarbanel, S. S.: The Interaction of an Oblique Shock Wave With a Laminar Boundary Layer. NASA MEMO 2-18-59W, 1959.

17. Abbott, Douglas E.; Holt, Maurice, and Nielsen, Jack N.: Investigation of Hypersonic Flow Separation and Its Effects on Aerodynamic Control Characteristics. ASD-TDR-62-963, U.S. Air Force, Nov. 1962. (Available from DDC as AD No. 296 112.)

18. Nielsen, J. N.; Lynes, L. L.; Goodwin, F. K.; and Holt, M.: Calculation of Laminar Separation With Free Interaction by the Method of Integral Relations. AIAA Paper No. 65-50, Jan. 1965.

19. Bogdonoff, S. M.; and Vas, I. E.: Some Experiments on Hypersonic Separated Flows. ARS J., vol. 32, no. 10, Oct. 1962, pp. 1564-1572.

20. Gray, J. Don: Laminar Boundary-Layer Separation on Flared Bodies at Supersonic and Hypersonic Speeds. AEDC-TDR-64-277, U.S. Air Force, Jan. 1965. (Available from DDC as AD 609841.)

21. Kaufman, Louis G., II; Hartofilis, Stavros A.; Evans, William J.; Oman, Richard A.; Meckler, Lawrence H.; and Weiss, Daniel: A Review of Hypersonic Flow Separation and Control Characteristics. ASD-TDR-62-168, U.S. Air Force, Mar. 1962.

22. Wuerer, J. E.; and Clayton, F. I.: Flow Separation in High Speed Flight — A Review of the State-of-the-Art. Rept. SM-46429, Missile & Space Syst. Div., Douglas Aircraft Co., Apr. 1965.

23. Kuehn, Donald M.: Laminar Boundary-Layer Separation Induced by Flares on Cylinders With Highly Cooled Boundary Layers at a Mach Number of 15. NASA TN D-2610, 1965.

24. Kuehn, D. M.; and Monson, D. J.: Boundary-Layer Separation and Reattachment With and Without Ablation. Separated Flows — Part I, AGARD CP No. 4, May 1966, pp. 121-145.

25. Rogers, E. W. E.; and Berry, C. J.: Research at the NPL on the Influence at Supersonic Speeds and Low Reynolds Numbers of Thick Laminar Boundary Layers. Rarefied Gas Dynamics, Vol. I, J. H. de Leeuw, ed., Academic Press, 1965, pp. 574-591.

26. Boatright, W. B.; Stewart, R. B.; and Sebacher, D. I.: Testing Experience and Calibration Experiments in a Mach Number 12, 1-Foot Hypersonic Arc Tunnel. Paper presented at Third Hypervelocity Techniques Symposium (Denver, Colorado), Mar. 1964.

27. Stewart, Roger B.: A Calorimeter Study of a Magnetically Stabilized Arc-Heater. AIAA J., vol. 2, no. 2, Feb. 1964, pp. 384-386.

28. Duckett, Roy J.; and Sebacher, Daniel I.: Velocity Measurements in the Langley 1-Foot (0.305-Meter) Hypersonic Arc Tunnel. NASA TN D-3308, 1966.

29. Guy, R. W.; and Winebarger, R. M.: Effect of Orifice Size and Heat-Transfer Rate on Measured Static Pressures in a Low-Density Arc-Heated Wind Tunnel. NASA TN D-3829, 1967.

30. Bertram, Mitchel H.; and Blackstock, Thomas A.: Some Simple Solutions to the Problem of Predicting Boundary-Layer Self-Induced Pressures. NASA TN D-798, 1961.

31. Cheng, H. K.; and Pallone, A. J.: Inviscid Leading-Edge Effect in Hypersonic Flow. J. Aeron. Sci. (Readers' Forum), vol. 23, no. 7, July 1956, pp. 700-702.

32. Kuehn, Donald M.: Blast-Wave Correlation of Pressures on Blunt-Nosed Cylinders in Perfect- and Real-Gas Flows at Hypersonic Speeds. AIAA J., vol. 1, no. 3, Mar. 1963, pp. 716-717.

33. Putnam, Lawrence E.: Investigation of Effects of Ramp Span and Deflection Angle on Laminar Boundary-Layer Separation at Mach 10.03. NASA TN D-2833, 1965.

34. Gray, J. Don: On the Existence of a Pressure Plateau in Pure Laminar Separated Flows. AIAA J., vol. 4, no. 8, Aug. 1966, pp. 1503-1504.

35. Erdos, John; and Pallone, Adrian: Shock-Boundary Layer Interaction and Flow Separation. Proceedings of the 1962 Heat Transfer and Fluid Mechanics Institute, F. Edward Ehlers, James J. Kauzlarich, Charles A. Sleicher, Jr., and Robert E. Street, eds., Stanford Univ. Press, c.1962, pp. 239-254.

36. Monaghan, R. J.: On the Behavior of Boundary Layers at Supersonic Speeds. Fifth International Aeronautical Conference, Inst. Aeron. Sci., Inc., June 1955, pp. 277-315.

37. Bertram, Mitchel H.; and Feller, William V.: A Simple Method for Determining Heat Transfer, Skin Friction, and Boundary-Layer Thickness for Hypersonic Laminar Boundary-Layer Flows in a Pressure Gradient. NASA MEMO 5-24-59L, 1959.

38. Holden, M. S.: Theoretical and Experimental Studies of Separated Flows Induced by Shock-Wave — Boundary-Layer Interaction. Separated Flows — Part I, AGARD CP No. 4, May 1966, pp. 147-180.

39. Miller, D. S.; Hijman, R.; and Childs, M. E.: Mach 8 to 22 Studies of Flow Separations Due to Deflected Control Surfaces. AIAA J., vol. 2, no. 2, Feb. 1964, pp. 312-321.

40. Johnson, Charles B.: Pressure and Flow-Field Study at Mach Number 8 of Flow Separation on a Flat Plate With Deflected Trailing-Edge Flap. NASA TN D-4308, 1968.

41. Moeckel, Wolfgang E.: Oblique-Shock Relations at Hypersonic Speeds for Air in Chemical Equilibrium. NACA TN 3895, 1957.

42. Moeckel, W. E.; and Weston, Kenneth C.: Composition and Thermodynamic Properties of Air in Chemical Equilibrium. NACA TN 4265, 1958.

43. Hansen, C. Frederick: Approximations for the Thermodynamic and Transport Properties of High-Temperature Air. NASA TR R-50, 1959. (Supersedes NACA TN 4150.)

44. Grabau, Martin: A Method of Forming Continuous Empirical Equations for the Thermodynamic Properties of Air From Ambient Temperatures to 15,000° K, With Applications. AEDC-TN-59-102 (Contract No. AF 40(600)-800), Arnold Eng. Dev. Center, Aug. 1959.